Chapter 3

Self-assembly of Nanoparticles into Membranes at the Liquid-Liquid Interface

3.1 Water/Toluene Interface Mediated Gold Nanoparticle-decorated Ultrathin Membrane by Ion-pair Formation

3.1.1 Introduction

Since the last decade, nanoparticle self-assembly processes at fluid interfaces have received considerable attention because of their importance encountered in separation and cleaning of oil, cosmetic preparation, waste water treatment and for storage and controlled delivery of various ingredients in the fields of medicine, pharmaceutics and agriculture.[1] About a century ago, Pickering discovered that finely divided colloidal solid particles could be adsorbed at the liquid-liquid interface to prevent the emulsion droplets behaving as a mechanical barrier against coalescence.[2] It is well-established in the literature that nanoparticles strongly segregate to the interface of immiscible fluids, driven by a reduction in interfacial energy.[3] Stabilization of nanoparticles at liquid-liquid interfaces by manipulating the particle surface energy offers tailor-made assemblies which have opened a new window to fabricate interfacially structured hybrid materials with unique properties.[4] However, while the nanoparticles are decorated with functional ligands for designing the hierarchical self-assembly, the assemblies can be stabilized and transformed into robust materials as the nanoparticles possess a range of surface-binding properties while the attached ligands can be tuned to tailor interaction with the surroundings. Based on this conceptive, nanoparticle-decorated membranes with sizes ranging from micrometers to millimeters have been designed with highly controllable permeability due to the presence of a close-packed layer of colloidal particles linked together to form a solid shell at fluid interfaces under benign reaction conditions. These systems features useful attributes, including, enhanced mechanical stability and controlled pore size distribution as well as the optical, fluorescent and magnetic properties depending on their precursor particles.[5-7] As a result, the application of this compatible chemistry is of great interest at the interface of materials science, chemistry and biology.[8-10]

A number of innovative strategies have been developed in the last few years with varieties of colloidal solid particles and versatility in ligand cross-linking chemistry to engineer nanoparticle-decorated membranes with diverse functionalities. Lin *et al.*[11] reported the cross-linking of the CdSe nanoparticles covered with reactive vinylbenzene in the presence of radical initiator at the water-toluene interface, creating ultrathin membranes and demonstrated the potential of

encapsulating water droplets across the membrane. Sastry and group[12] have described the organization of nanoparticles of gold into two-dimensional superstructures at the water-chloroform interface between the gold hydrosol and benzene/anthracene in chloroform. Duan *et al.*[13] have successfully implemented interfacial self-assembly of Au and Fe_3O_4 nanoparticles by capping them with ligands bearing a 2-bromo 2-methylpropionate termini. Rotello and co-workers[14] have reported the fabrication of membranes by cross-linking terpyridine thiol-functionalized FePt nanoparticles through complexation of terpyridine with Fe(II) metal ions at the water-toluene interface. He *et al.*[15] have demonstrated a drying-mediated self-assembly process that can be used to create close-packed monolayer membranes that span holes tens of micrometer in diameter. To meet the challenges that lie ahead, there is an increasing interest to develop organizational strategy for nanoparticles at liquid-liquid interfaces through self-assembly processes at the two-dimensional level leading to the formation of novel membranes for real-time applications.

In this section, we have demonstrated a simple and facile approach for the fabrication of nanoparticle-decorated ultrathin membrane by performing interfacial self-assembly of the functionalized nanoparticles at the liquid-liquid interface. The composite organic-inorganic, nanometer-thick membrane has shown promise to allow the diffusion of small molecules across the interface.

3.1.2 Experimental

3.1.2.1 Synthesis of Mercaptoundecanoic Acid-Stabilized Gold Nanoparticles

Gold nanoparticles were synthesized following the method reported by Shi *et al.*[16] An amount of 0.044 g 11-mercaptoundecanoic acid (11-MUA) dissolved in 5 ml of methanol was added to 10 ml of 10 mM methanolic solution of $HAuCl_4$ under vigorous stirring on a magnetic stirrer. The solution turned milky white after mixing and was continued further. After 20 min, 5 mL of freshly prepared 0.3 M ice-cold aqueous sodium borohydride was added to the mixture dropwise with stirring. The mixture, immediately, turned deep brown indicating the formation of Au nanoparticles. The stirring was continued for 1 h. The functionalized gold particles so formed were precipitated from methanol by centrifugation at 10,000 rpm for 10 min and were subsequently redispersed in water. The surface plasmon oscillation of the gold particles show the absorption band at *ca.* 520 nm and the particle size was measured as 3±0.6 nm from TEM

measurements. The gold nanoparticles prepared by this method are stable for a couple of weeks and can be stored under ambient condition for several days without any significant agglomeration or precipitation between the particles.

3.1.2.2 Fabrication of Gold Nanoparticle-Decorated Ultrathin Membrane at the Water-Toluene Interface

The cross-linking between the ligand-covered gold nanoparticles and cetylpyridinium chloride at the water-toluene interface for the fabrication of membrane can be described as follows. An aliquot of 2 mL of aqueous dispersion of gold nanoparticles (0.1 mM) and 2 mL of cationic surfactant, cetylpyridinium chloride (0.1 mM) in toluene was taken in a test tube and shaken vigorously. Now, an aliquot of 0.1 mL of a weak base, K_2CO_3 (0.1 M) was added to the test tube and shaken well. It is seen that the gold nanoparticles undergo swift movement at the interfacial region and form a homogeneous membrane at the liquid-liquid interface.

3.1.3 Results and Discussion

A schematic presentation of the formation of the nanoparticle-decorated membrane is depicted in Scheme 3.1.1. In this investigation, we have selected gold nanoparticle as the core material for

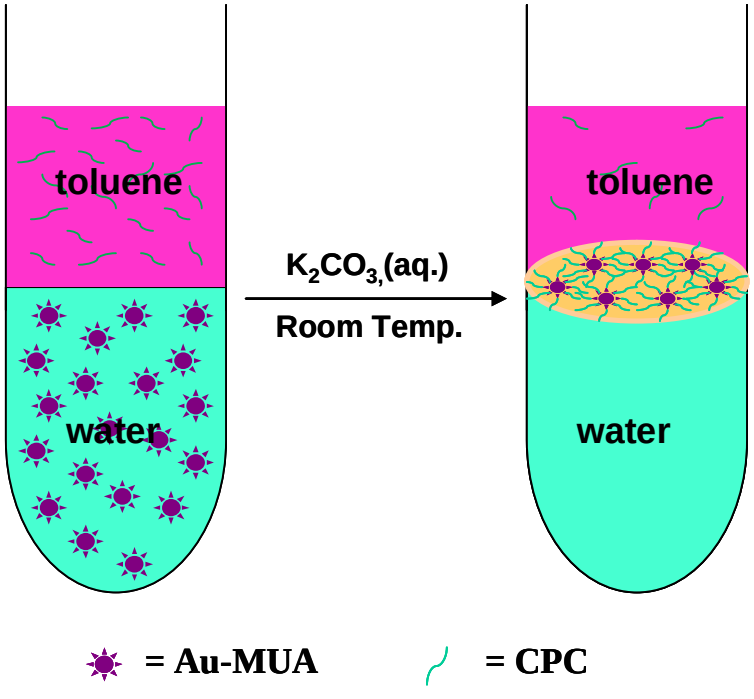

Scheme 3.1.1. Schematic presentation showing the formation of nanoparticle-decorated membrane at the water-toluene interface.

the binding of bifunctional surfactants onto the particle surface. It is well-established in the literature that gold binds to –SH group rather than carboxylic acid group of 11-MUA due to higher polarizability of sulfur than oxygen.[17-19] This renders gold nanoparticles stabilized by thiol group and carboxylic acid group pointing outwards the particle surface that provides chain-end functional groups for subsequent reactivity. When cationic surfactant, CPC is added to the toluene layer and subsequently, upon addition of the weak base, the proton of the carboxylic acid group is abstracted and there is ionic interaction between the carboxylate of 11-MUA bound to the gold surface and pyridinium cation of CPC leading to the formation of cross-linked nanoparticle assembly at the water-toluene interface. However, in the absence of the base, the nanoparticles undergo phase separation so as to form a separating layer between the water and toluene and there is no formation of the membrane. The ultrathin membrane formed by this method is stable for a week without any significant rupturing and remain dispersed until the membrane is suspended at the water-toluene interface. The images of the membrane composed of gold nanoparticles are shown in Figure 3.1.1. Figure 3.1.1A shows the digital camera

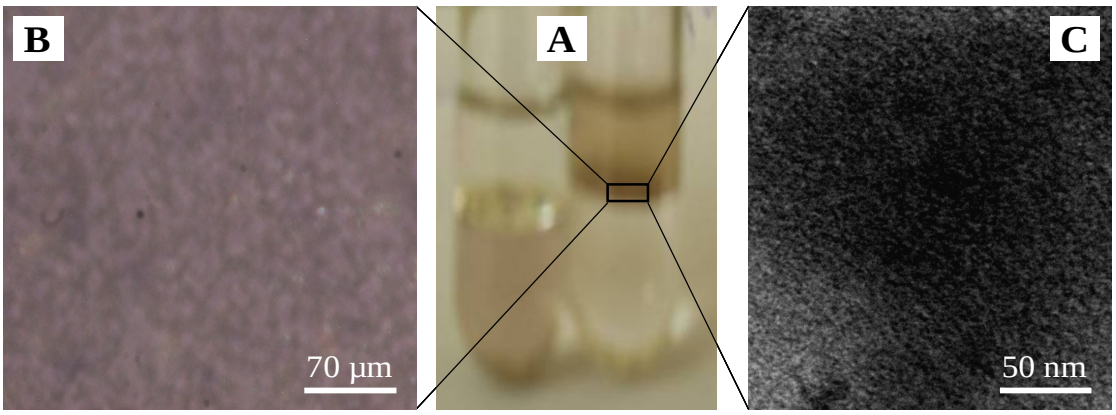

Figure 3.1.1. (A) Digital camera photograph of the separated aqueous and organic layer and that of after the formation of nanoparticle-decorated membrane at the water-toluene interface; (B) dark-field optical microscopic image of a portion of the membrane on the glass slide and (C) transmission electron microscopic image of the membrane dried in air on carbon-coated copper grid.

photograph of the two layers before and after formation of the membrane. Before the formation of the membrane, the aqueous layer is seen red due to the presence of gold nanoparticles and the toluene layer containing CPC appears light yellow. It is seen that both the aqueous and toluene

layer is clear at the naked eye after formation of the membrane at the interface. The opaque red appearance of the toluene layer after membrane formation is due to the reflection of light from the membrane at the interface. Optical micrograph of a portion of the membrane under dark field is shown in Figure 3.1.1B recorded by a typical transmission light method. The membrane was removed from the interface by micropipet and suspended in toluene on the cavity of a glass slide. The optical microscope image of the membrane indicates a thin-film morphology consisting of well-ordered, close-packed particle assembly. The observation of a structurally intact membrane floating freely in toluene demonstrates that the ligands attached to the nanoparticles are cross-linked into a continuous membrane. The slight crumpling on the morphology may result from shear stresses during manipulation of the membrane with the micropipet and partially due to drying on the glass slide. Figure 3.1.1C shows the transmission electron microscopic image of the membrane dried in air on a carbon-coated copper grid. At high magnification, individual gold nanoparticles are seen which identify that the membrane is composed of multiple shells of closely packed 3 nm gold particles with liquid-like ordering.[11] The interstitial space in these nanoparticle-based materials points out to the possibility to provide ideal channels to restrict or control the diffusion of the active core ingredients across the capsule wall.

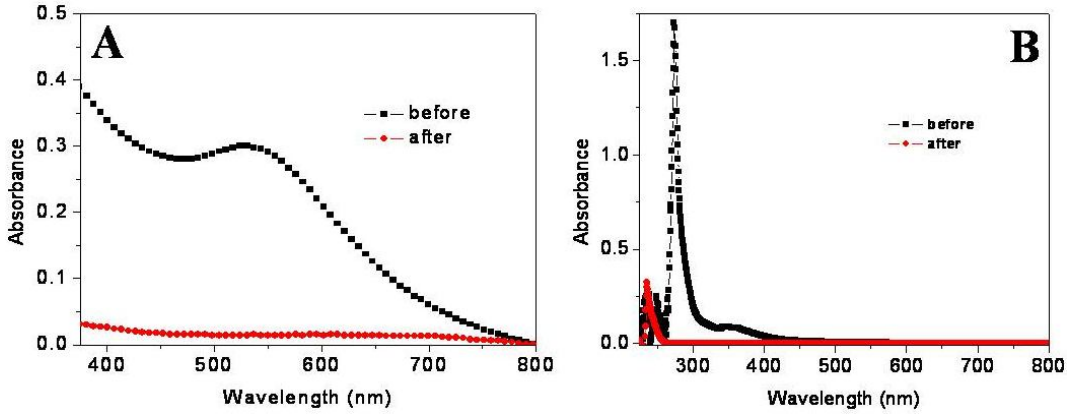

Figure 3.1.2. Absorption spectra of (A) gold nanoparticles in aqueous medium before and after the formation of the membrane at the liquid-liquid interface; (B) CPC in toluene before and after the formation of the membrane at the liquid-liquid interface.

The formation of the nanoparticle-decorated membrane constituted of gold nanoparticles at the liquid-liquid interface could be monitored by UV-vis spectroscopy (Figure 3.1.2). In graph A, it is seen that aqueous solution of gold nanoparticles shows the surface plasmon absorption with

maximum at 520 nm. After the formation of the membrane, the plasmon band of gold is almost vanished indicating the participation of the gold nanoparticles in the formation of the membrane. Graph B shows absorption spectrum of CPC in toluene with an absorption maximum at 283 nm. After formation of the membrane, the intensity of CPC band is significantly reduced indicating that a large fraction of CPC molecules are involved in the formation of the membrane and a smaller fraction is present in the organic phase at thermodynamic equilibrium.

The formation of the membrane due to ionic interaction in the presence of a weak base between the gold nanoparticles bearing a negatively charged surface pointing outwards with the cationic surfactant, cetylpyridinium chloride was confirmed by FTIR spectroscopy. The FTIR

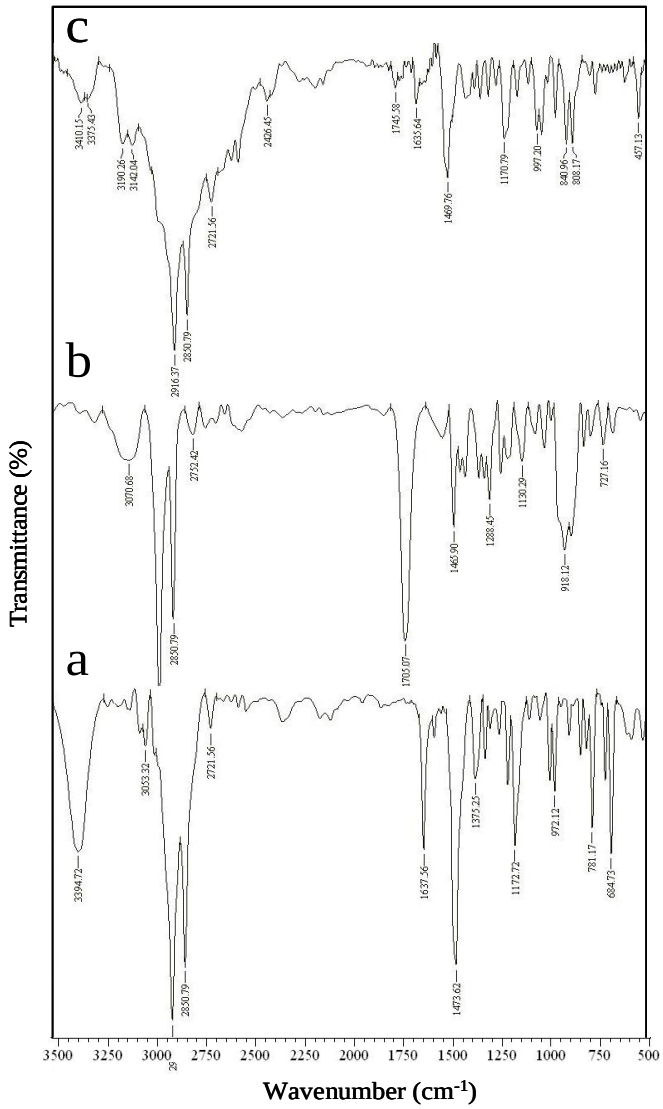

Figure 3.1.3. FTIR spectra of (a) CPC, (b) 11-MUA stabilized gold and (c) nanoparticle-decorated membrane.

spectra of CPC, 11-MUA stabilized gold and nanoparticle-decorated membrane on KBr pellets are shown in Figure 3.1.3. The characteristic FTIR absorption peak of CPC with $-N^+$ at 1637 cm^{-1} is shown (trace a) concomitant with earlier studies.[20] Although the carboxylic carbonyl stretch C=O appears as an intense band at 1705 cm^{-1} and -OH stretch appears as a very broad band centred at about 3070 cm^{-1} are seen, the absence of weak S-H absorption peak at around 2500 cm^{-1} (trace b) gives clear evidence that 11-MUA anchors the gold surface through the sulfur atom of the mercapto group as has been seen in earlier studies.[21] After complexation with CPC, the characteristics -OH absorption peak of 11-MUA at 3070 cm^{-1} and $-N^+$ absorption peak at 1637 cm^{-1} is significantly reduced, indicating the formation of an ion-pair between $-N^+$ of pyridine with the $-COO^-$ ion of carboxylic acid in the presence of base (trace c).[20,22]

Since the membrane was fabricated by performing interfacial cross-linking of the associated ligand molecules around the nanoparticles and the CPC molecules, their permeability is expected to be determined by the sizes of the interstices between the nanoparticles assembled on the membrane wall. To demonstrate the membrane wall permeablity, we have studied the release of water-soluble fluorescein isothiocyanate (R_h = 0.54 nm) (FITC) across the membrane. After the membrane formation, a droplet of an aqueous solution of FITC was placed on top of the membrane. Figure 3.1.4 shows the membrane's ability to trapping or adsorption of particles

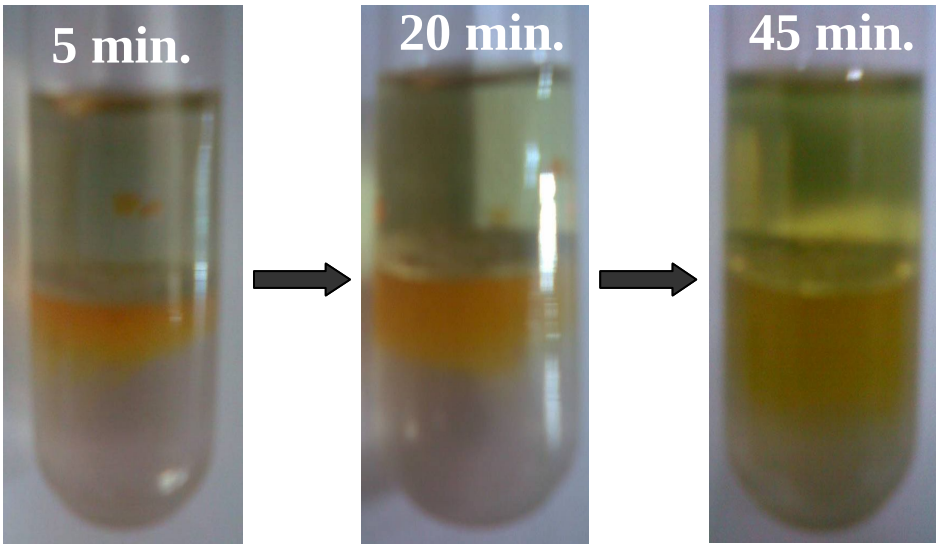

Figure 3.1.4 Digital camera photographs of dye (red solution) becoming entrapped and then diffusing across the membrane of cross-linked nanoparticles. The bold arrow points to the interface in each tube.

within the membrane and increase the diffusion time of permeating substances. After ~2 min, the dye molecules start to penetrate and slowly diffuse into the aqueous phase. In general, transport through a membrane can be described as arising from two contributions: diffusion due to concentration gradients (J_C) and convection due to pressure gradients (J_D) and the total flux J is, therefore, given by $J = J_C + J_D$.[23] Under ambient condition, the transport is likely to be dominated by diffusion due to concentration gradients. It is noted that the diffusion front of the dye in water is fairly sharp, indicating an absence of convection current in the aqueous phase. In control experiments, using non-crosslinked assemblies of the gold nanoparticles, the dye molecules penetrated the nanoparticle assembly by convection within few seconds and spread over the entire aqueous phase. These results point to the robust barrier properties of the nanoparticle membrane and their ability to prevent convective mixing without any mechanical deformation of the membrane wall. In contrast, two high molecular weight fluorescein isothiocyanate-functionalized dextran polymer (MW ~ 40,000 g mol^{-1}, R_h = 3.7 nm and MW ~ 5,00,000 g mol^{-1}, R_h = 9.4 nm) could not diffuse across the membrane. This phenomenon shows that the membrane is permeable, yet may serve to retard or suppress the diffusion of larger molecules across the layer. Thus, the permeable and robust membrane indicates their potential as diffusion barriers. If the membrane is assumed to be a shell of perfect hexagonal lattice of spheres of diameter d, the interstitial holes are roughly 0.15d in size.[24] Assuming the particle size as ~3.0 nm in the present experiment, the interstitial holes are set approximately 0.45 nm. The permeability of the interstitial holes might be further reduced by the additional layers and would also help to mitigate effects of any defects in the lattice of the particles. Therefore, it is seen that the membrane composed of 3.0 nm particles allows 0.54 nm FITC molecules but completely impermeable to FITC-functionalised dextran polymers. These results demonstrate that selective permeability of colloidomes can be readily achieved in consistent with the simple geometric model for the permeability.

3.1.4 Conclusion

In summary, self-assembly of chemically functionalized plasmonic gold nanoparticles at the water-toluene interface, coupled with chemical cross-linking of the attached ligands based on the formation of ion-pair in the presence of a weak base, provides a simple and flexible route for the

fabrication of robust and oil-soluble nanoparticle-decorated organic-inorganic hybrid membrane at the water-toluene interface. Interfacial cross-linking of the nanoparticles at the interface enables the encapsulation of selective water-soluble dye molecules showing the permeability of the nanostructured membrane. In order to increasing possibilities of the membranes for real-time applications, the two-dimensional organised nanoparticle assemblies also provide new and convenient model system to evaluate long-range mediated interactions of the small particulates at interfaces. Finally, by proper choice of the constituent nanoparticles, these assemblies can be modulated to various magnetic, fluorescent and photonic materials. A simple and facile route is presented to fabricate robust membrane based on the interfacial self-assembly of 11-mercaptoundecanoic acid-covered gold nanoparticles and cetylpyridinium chloride in the presence of a weak base at the water-toluene interface. Observation of the interfacial self-assembly by microscopic techniques demonstrates the formation of nanoparticle-decorated ultrathin membrane composed of close-packed nanoparticles with liquid-like ordering. The ion-pair formation between 11-mercaptoundecanoic acid-covered gold nanoparticles and cetylpyridinium chloride in the presence of a weak base has been confirmed by UV-Vis and FTIR spectroscopy. The formation of structurally intact membrane at the interface enables the encapsulation of selective water-soluble dye molecules exhibiting permeability for real-time applications.

3.2 Water/CCl_4 Interface-mediated Au-ZnO Composite Membrane using 'Thiol-Ene' Click Chemistry

3.2.1 Introduction

In recent years, self-assembly processes based on selective control of non-covalent and covalent interactions[25] for synthesizing nanoparticle-decorated membranes (2-D) and capsules (3-D) at fluid interfaces has attracted researchers due to their potential applications in controlled encapsulation and release.[1,26-27] A variety of cross-linking strategies have been pursued for designing two-dimensional arrangement of both hydrophilic and hydrophobic nanoparticles at oil-water interfaces.[24,28,29] However, Sharpless visionary characterization of several idealised reactions as click reactions, the materials science and synthetic chemistry community have, often, preferred the exploitation of click chemistry (which describes a number of simple, modular, and highly specific chemical reactions featuring high yields under mild conditions) in comparison with traditional coupling strategies.[30] First, click chemistry involving 'thiol' and 'ene' functional groups is highly selective and essentially inert to many functional groups and environmental conditions (e. g., pH and solvent). Second, the click chemistry approach provides dense packing of the nanoparticles and stronger network due to formation of covalent bonds

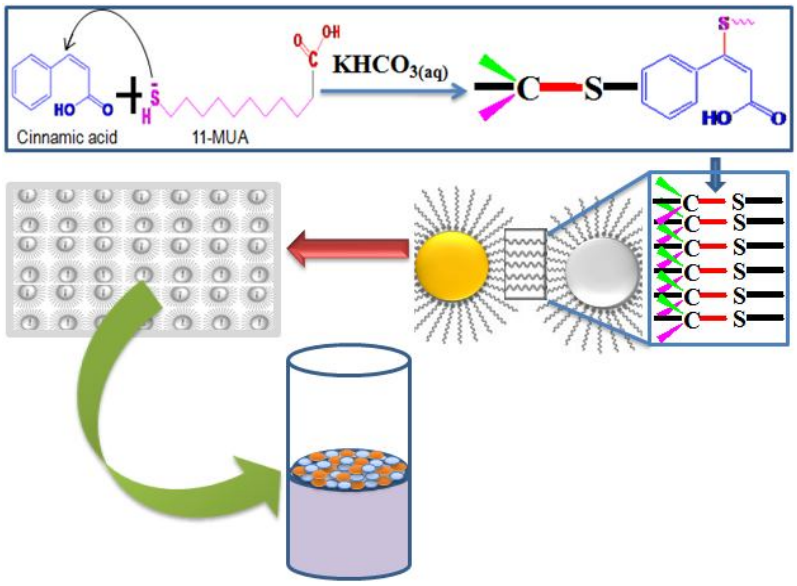

Scheme 3.2.1 Schematic representation of synthesis and filtration application of click mediated membrane

amongst the ligands at the liquid-liquid interface, resulting in high stability of the membranes. Although, copper catalysed Huisgen 1,3-dipolar cycloaddition reaction of organic azides and alkynes has been the most employed in this field,[31] the introduction of 'thiol-ene' click chemistry (introduced by Charles Goodyear in the mid of 19th century for the vulcanisation of natural rubber[34] has shown impressive versatility for overcoming long-time synthetic challenges. The flexibility of thiol-ene click chemistry allows for the preparation of well-defined materials in polymer and materials science, organometallic chemistry, chemistry of peptides, and molecular biology.[32-34] To illustrate some of these breakthroughs, thiol-ene reaction has been utilised for network formation, polymer functionalization, dendrimer synthesis, and the decoration of two- and three-dimensional objects in numerous fields, e. g., functionalization of porous polymer monoliths, soft imprint lithography, synthesis of functionalised peptides, radiopharmaceutical coupling of a radioactive metal complex with a biological targeting molecule and their computational and kinetic analysis.[33-35] Rotello and colleagues have elegantly employed 1,3-dipolar cycloaddition of azide- and alkyne- functionalised Fe_3O_4 nanoparticles in the presence of copper catalyst for the formation of magnetic capsules at water-oil interface.[36]

In this section, we have described the fabrication of composite membrane, made up of zinc oxide (ZnO) and gold (Au) nanoparticles, by performing 'thiol-ene' click reaction between the thiol group of 11-MUA anchored onto ZnO nanoparticle surface and ene functionality of cinnamic acid attached onto gold nanoparticle surface, in the presence of catalytic amount of weak base. The formation of the nanoparticle-decorated membrane has been characterized by UV-visible spectroscopy, Fourier transform infrared spectroscopy, transmission electron microscopy, scanning electron microscopy, atomic force microscopy, and optical and fluorescence microscopic images. The permeability of the membrane has been examined using five amino acids (*viz.*, glycine, alanine, valine, isoleucine and proline corresponding to isoelectric points (IP) as 6.06, 6.11, 6.00, 6.05 and 6.30 respectively) at different charge states corresponding to different pH conditions of the solution.

3.2.2 Experimental

3.2.2.1 Synthesis of Gold Nanoparticles

The 11-mercaptoundecanoic acid-stabilized ZnO nanoparticles were synthesized in an one-pot reaction using methanol as the solvent by following the procedure of Weller group.[37] An

aliquot of 0.055 g $Zn(OOCCH_3)_2.2H_2O$ was dissolved in 25 mL of methanol in a double-necked round-bottom flask by refluxing the mixture for 45 min on a water bath at 45 °C. Subsequently, 1.36 g 11-MUA was added to the solution and refluxing was continued for another 30 min. After that, the temperature was increased to 60 °C, 13.5 methanolic solution of KOH (0.1 mM) was added instaneously and continued for another 2 h. The color of the solution became curdy white indicating the formation of zinc oxide nanoparticles. Then, the heating was stopped and the mixture was stirred for 12 h at room temperature. The 11-MUA functionalized ZnO nanoparticles so obtained were retrieved from methanol by repeated centrifugation at 10,000 rpm for 15 min and washing with water 3-4 times and were, subsequently, redispersed into water. The dispersion was found to be stable for several days while stored in the dark.

3.2.2.2 Synthesis of Gold Nanoparticles

Cinnamic acid-stabilized gold nanoparticles were synthesized by following the procedure reported by Wang *et al.*[38] To an aliquot of 9.75 mL ethanolic solution of cinnamic acid (1.0 mM), 0.25 mL $HAuCl_4$ (0.25 mM) solution was added with constant stirring. Then, 1.0 mL ice-cold aqueous solution of $NaBH_4$ (20 mM) was added dropwise into the mixture and stirring was continued for another 30 min. The colour of the solution becomes red indicating the formation of gold nanoparticles. The cinnamic acid stabilized gold nanoparticles so obtained were retrieved from ethanol by repeated centrifugation at 10,000 rpm for 15 min and washing with water 3-4 times and were, subsequently, redispersed into water. The nanoparticles prepared by this method are stable for a couple of weeks without any significant agglomeration or precipitation of the particles.

3.2.2.3 Preparation of the Membrane

In this experiment, 11-mercaptoundecanoic acid (11-MUA) stabilized ZnO and cinnamic acid-stabilized Au nanoparticles have been prepared with average particle sizes as 3±0.5 nm and 5±0.7 nm respectively. These ligand-stabilized nanoparticles have been exploited for designing composite membrane at aqueous-organic interface by ligand cross-linking. In a test tube, an aliquot of 1.5 mL ZnO (0.003%, volume fraction) and 1.5 mL Au NPs (0.003%, volume fraction) were mixed together and 3 mL CCl_4 was placed beneath the aqueous layer. Now, catalytic amount of weak base, $KHCO_3$ was added with vigorous shaking and then, allowed to

settle. It is seen that both the nanoparticles get adsorbed and self-assembled at the interface resulting in the formation of membrane at the liquid-liquid interface.

3.2.2.4 Studies on the Permeability of the Membrane

To analyze the charge-dependence of the solute molecules to permeate across the membrane, five different amino acids, *viz.*, glycine, alanine, valine, isoleucine and proline were employed to pass through the membrane under different pH conditions. It is well known that, the amino acid molecules are neutral at its isoelectric point (PI), positively charged below its isoelectric point and negatively charged above the isoelectric point respectively. When pH<PI, i. e, medium is acidic, the $–NH_2$ group of amino acid will accept a proton and become positively charged ($-NH_3^+$) and alternatively, in alkaline medium (pH>PI), due to the formation of $–COO^–$, the amino acid become negatively charged. In this experiment, after formation of the membrane at the water-oil interface, amino acid solutions were allowed to pass through the membrane at pH = PI for neutral molecules and pH = PI ± 0.5 for charged state. When, amino acid molecules will pass through the membrane due to concentration gradient, it will come in contact and react with ninhydrine and will produce intense blue colour. An aliquot of amino acid solutions of desired pH (adjusted prior to mixing by adding acetate buffer, the overall ionic strength due to the addition of buffer solution is in the range of ~0.015 M) was injected into the CCl_4 layer (at the bottom of the test tube) by a syringe fitted with a sharp needle through the side of the test tube and ninhydrin solution was added into the aqueous layer (on the top of the test tube) slowly. It is to be remembered that if the needle is inserted through the membrane, the hole created would allow amino acid molecules to pass through before its mitigation, which might lead to the development of faint coloration in case of charged state. Since, in the present experiment, the needle was inserted carefully through the side of the test tube, therefore, small hole or channel created in this process will automatically be compensated and would not affect the diffusion process seriously. The concentration of both amino acid and ninhydrin solution (maintained at 0.01 M) and incidentally, the pH of the solution is adjusted already in the range which is reported concentration and pH for the reaction between amino acids and ninhydrin to take place.

3.2.3 Results and Discussion

In this experiment, 11-mercaptoundecanoic acid stabilized ZnO and cinnamic acid-stabilized Au nanoparticles have been prepared with average particle sizes as 3±0.5 nm and 5±0.7 nm respectively. These ligand-stabilized nanoparticles have been exploited for designing composite membrane at aqueous-organic interface by ligand cross-linking. In a test tube, an aliquot of 1.5 mL ZnO (0.003%, volume fraction) and 1.5 mL Au NPs (0.003%, volume fraction) were mixed together and 3 mL CCl_4 was placed beneath the aqueous layer. Now, catalytic amount of weak base, $KHCO_3$ was added with vigorous shaking and then, allowed to settle. It is seen that both the nanoparticles get adsorbed and self-assembled at the interface resulting in the formation of membrane at the liquid-liquid interface. The fabrication of the membrane was tried with several other water-immiscible solvents, *viz.*, benzene, toluene, *n*-hexane, *n*-heptane, dichloromethane, $CHCl_3$ and CCl_4. It was observed that the membrane formation occurs selectively for four solvents, *viz.*, $CHCl_3$, CCl_4, toluene and *n*-hexane. However, the homogeneity of the membrane is the best achieved in case of CCl_4. This is due to the fact that the position of colloidal particles at the water-oil interface is determined by their contact angle: for a hydrophilic particle with a contact angle smaller than 90^0, its larger fraction resides in the water bulk phase, or vice versa. As particles scale down to the nanometer size, however, the thermal energy becomes comparable to the interfacial energy. In this case, spatial fluctuations suffice to remove NPs trapped at interfaces into bulk phases. Therefore, it could be suggested that water-CCl_4 interface prefers the entrapment of all particles offering viable platform for the formation of the membrane.[39] The formation of the composite membrane at the interface from its individual constituents could be followed by UV-vis spectroscopy as shown in Figure 3.2.1. All the absorption spectra were measured in the solid state. The absorption spectrum of ZnO NPs shows a sharp absorption peak at 276 nm and a less intense band at 330 nm that appear corresponding to interband (valance band to conduction band) and intraband (donor/acceptor impurity level to conduction level) transitions respectively.[40] The absorption spectrum of Au NPs exhibits a characteristic surface plasmon oscillation of the conduction electrons coherent with incident electromagnetic radiation.[41] The other broad band at 298 nm is due to π-π^* transition of cinnamic acid molecules attached onto the gold surface.[42] The ZnO-Au composite membrane shows the red-shifting of the surface plasmon band of Au and blue shifting of the absorption maximum of ZnO NPs indicating electronic interaction between the nanoparticles in the membrane.[41, 43] Inset shows the digital

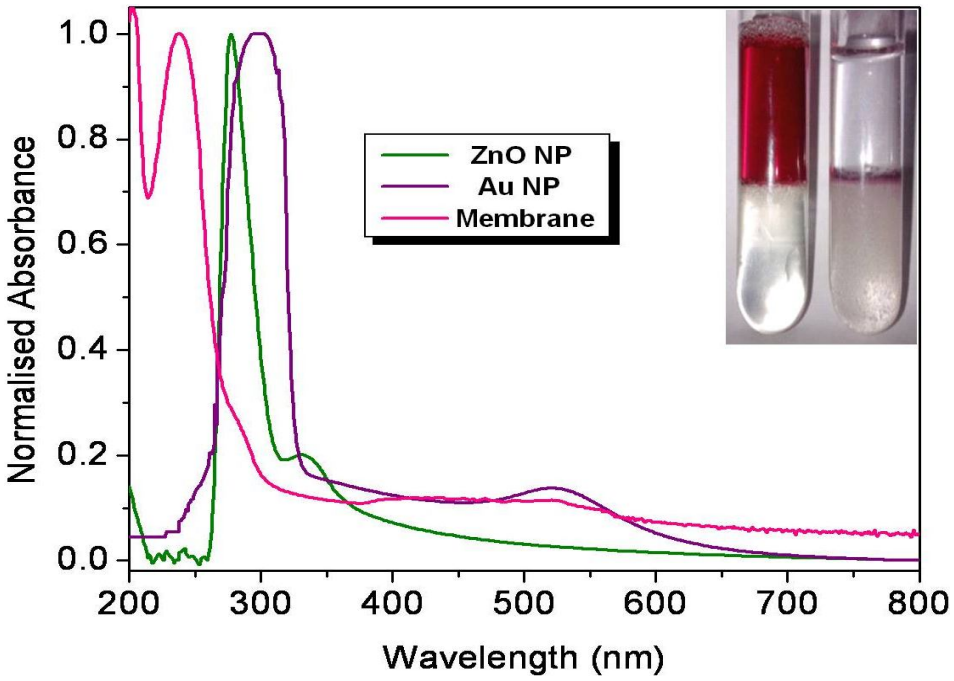

Figure 3.2.1. UV-vis spectra (measured in the solid state) of individual nanoparticles and composite membrane. Inset shows the digital camera photograph before and after membrane formation.

camera photograph of the formation of the membrane at the aqueous-organic interface. Before the formation of the membrane, the aqueous layer is seen red containing both ZnO and Au nanoparticles. After shaking in the presence of weak base, a reddish impression at the liquid junction indicates the formation of the membrane at the interface.

All the spectra of the samples were measured in the solid state. Before the formation of the membrane, the substrate contained only ZnO and gold nanoparticles at a particular concentration. In the membrane, the concentration of gold is lower than that of the only gold situation and moreover, due to the presence of ultrasmall ZnO particles in the interim in the membrane, there is electromagnetic coupling effect between the gold particles and as a result, the spectrum is broadened.[41]

Successful 'click reaction' between the terminal thiol functionality of 11-MUA anchored onto the ZnO NPs through –COOH group and ene functionality of cinnamic acid anchored onto the Au NPs was confirmed by Fourier transform infrared spectroscopy (Figure 3.2.2). Before click reaction, the characteristic –S–H stretching peak at 2574 cm^{-1} (panel a) and –C=C– peak at 1625 cm^{-1} (panel b) are clearly observed. After the reaction, these peaks are almost vanished

indicating successful 'click reaction' between the ligands attached onto nanoparticle surface.[44] In a control experiment, no decrease in the relative peak intensity was observed in the presence of either Au or ZnO particles and the catalyst. Therefore, it could be inferred that, in the presence of the weak base, 'thiol-ene' click reaction between terminal thiol group of 11-MUA and double bond moiety of cinnamic acid takes place (a Michael addition-type reaction) as shown in Scheme 3.2.2. It is pertinent, here, to mention that these membranes are usually formed either due to

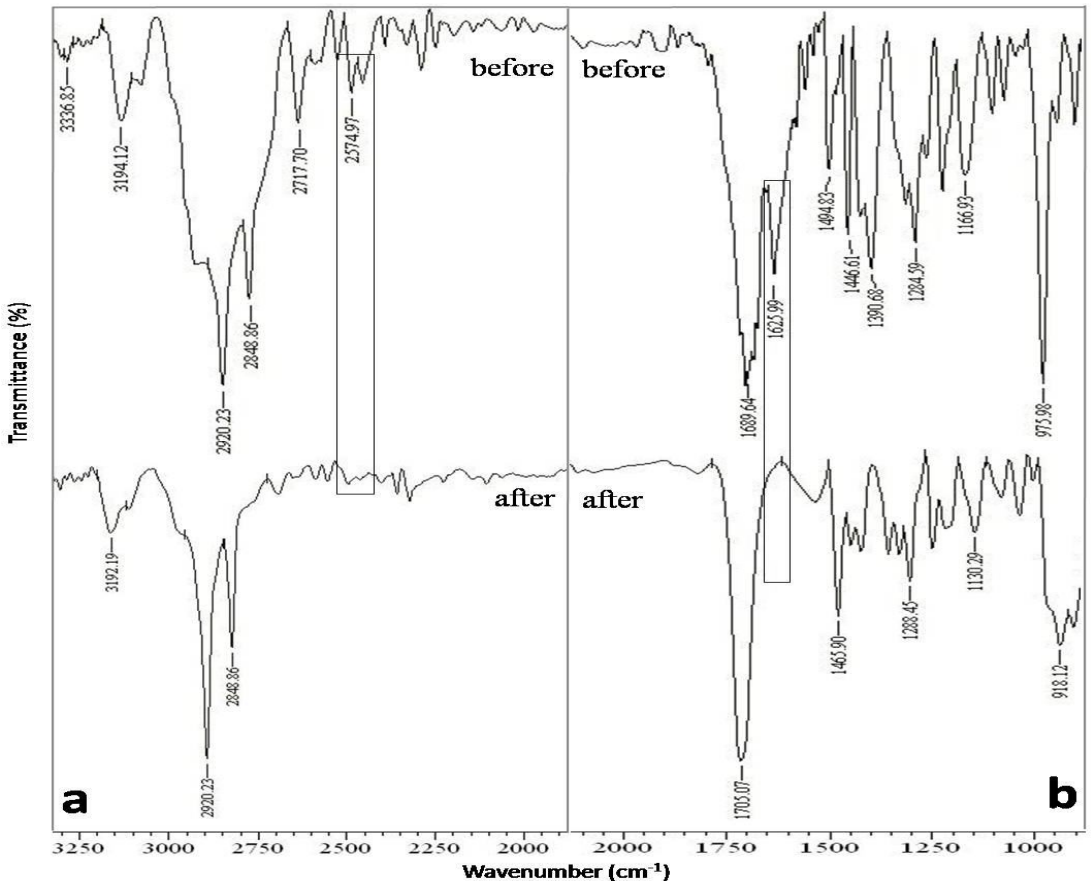

Figure 3.2.2. FTIR spectra of (a) 11-MUA stabilized ZnO nanoparticles, and (b) cinnamic acid stabilized gold nanoparticles, before and after formation of the membrane.

interdigitation of ligands or through ligand cross-linking or due to van der Waals' attraction.[24,28,29] In the present experiment, a covalent bond is formed between the attached ligands of ZnO and Au NPs, referred as 'thiol-ene' click reaction. As a result, the forces responsible for holding the nanoparticles together are very strong and such covalently bonded membrane possess high mechanical strength.

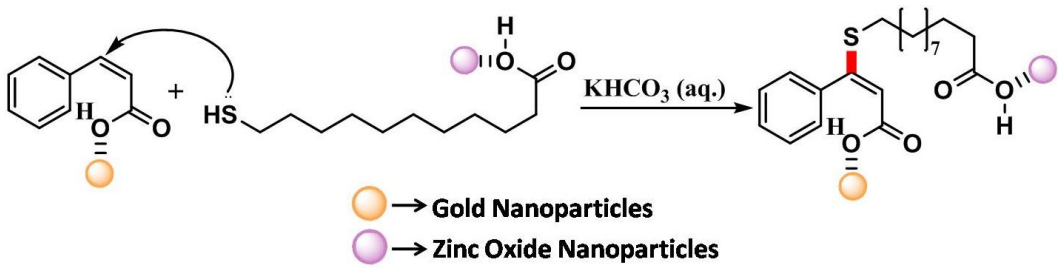

Scheme 3.2.2. Schematic presentation of the 'thiol-ene' click reaction (Michael-like addition) for the formation of nanoparticle-decorated membrane.

The images, composition and thickness of the nanoparticle-decorated composite membrane are presented in Figure 3.2.3. Panel (a) and (b) show the optical (recorded by a typical transmission light method) and fluorescence (excitation: 276 nm, detection: 603 nm) micrographs (under bright field) respectively of a portion of the membrane. The membrane was removed from the interface using a micropipet and suspended in CCl_4 on the cavity of a glass slide. The microscopic image shows the impression of a thin film-like structure of the membrane. Representative TEM image of the membrane presented in panel (c) exhibits that the membrane is composed of Au and ZnO nanoparticles with liquid-like ordering.[11] In the image of the membrane, the Au NPs appear dark and ZnO NPs are light coloured because gold has a

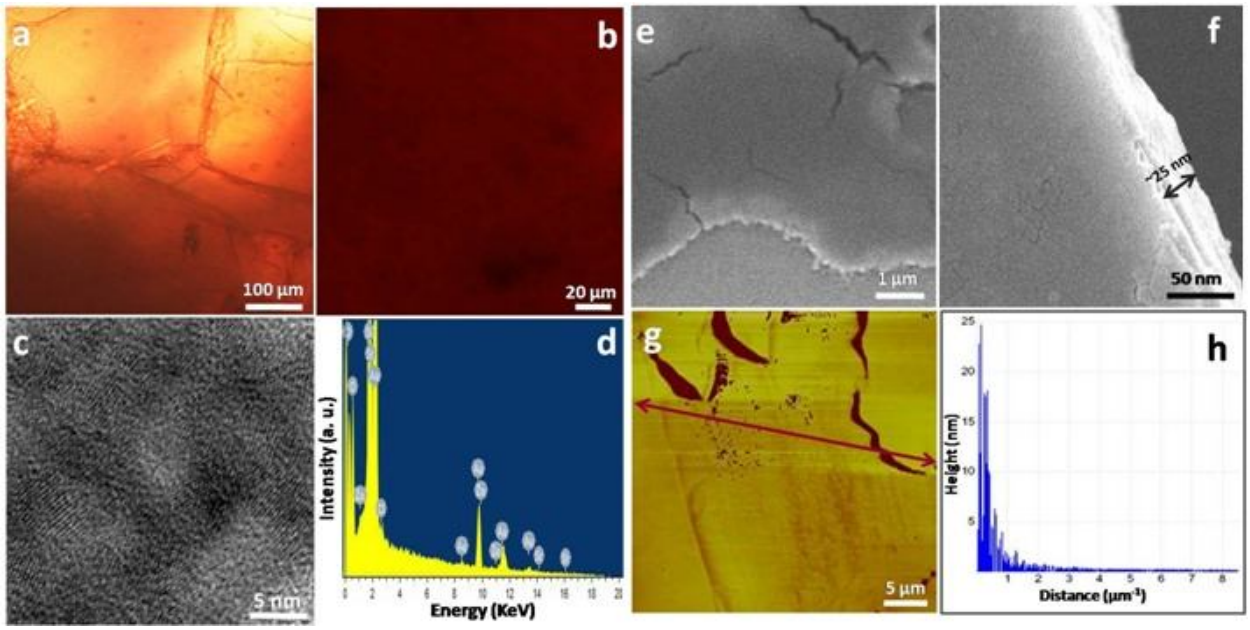

Figure 3.2.3. (a) Optical and (b) fluorescence micrograph; (c) transmission electron micrograph and (d) energy dispersive X-ray spectrum; (e) top-view and (e) side-view of the scanning electron micrograph; and (g) atomic force micrograph (h) step height along the line indicated on the surface of the membrane.

higher electron density and allows fewer electrons to transmit.[41] The energy dispersive X-ray spectrum (panel d) reveals that the particles are composed of Zn, Au and O elements which comes from the ZnO and Au particles. The mole ratio of Au and Zn in the membrane is *ca.* 1.0 : 0.943. The crumpling on the morphology may result from shear stresses during manipulation of the membrane with the micropipet on the TEM grid. Panel (e) and (f) represent the top-view and side-view of the SEM images illustrating the surface morphology and thickness of the membrane onto the silicon wafer. The observation of a structurally intact membrane (cracks appear due to drying of the solvent onto the wafer surface) demonstrates that the ligands attached to the nanoparticles are cross-linked into a continuous membrane. The side-view indicates that the membrane is composed of multiple layers of nanoparticles. Representative AFM image in panel (g) renders an idea about the surface roughness of the membrane onto the silicon wafer. Direct measurement of the thickness (panel h) of the assembled layer of the membrane could be pursued from AFM study. From the one-dimensional power spectral density function plot, the height distribution curve shows that the average height of the membrane from the substrate is approximately 25 nm, which is slightly higher than that expected for a membrane perfectly covered with a monolayer of particles (assumed to be *ca.* 10 nm corresponding approximately to the diameter of the nanoparticles and their associated ligand molecules). A plausible explanation for this variation in the height distribution may be related to that the membrane is composed of multiple layers of densely packed nanoparticles (may arise to counterbalance the surface energy of both ZnO and Au NPs) as has been seen in prior studies[45] along with the roughness created due to drying of the membrane on the wafer.

Now, we have attempted to elucidate the permeability of the composite membrane made of ultrasmall ZnO and Au nanoparticles. The permeability of a membrane is governed by the size and shape of the constituent particles, osmotic pressure of the pores (i. e., gradients of pressure that originate from concentration gradients at the pore) and thickness of the porous wall and these factors could be tuned according to the specific application.[46] Wang *et al.*[47] have observed that 5.0 nm Fe_3O_4 nanoparticle-decorated capsules selectively release 2.8 nm CdTe NPs and keep 4.0 nm CdTe NPs inside during storage in water because their cut-off is 3.5 nm, in between small and large CdTe NPs. Jaeger and colleagues[23] have found 1.65 nm mean pore diameter with 5±0.5 nm particles and objects with cross-section larger than 1.7 nm are rejected completely. It

was also observed that filtration coefficients of 2 orders of magnitude higher for nanoparticle membranes than those observed in polymer-based filters in case of aqueous solution of some selective solute molecules. In this experiment, if the membrane is assumed to be a shell of perfect hexagonal lattice of spheres of diameter d, the interstitial holes are roughly 0.15d in size.[24] Assuming the average particle size as ~5.0 nm for both Au and ZnO, the interstitial holes are set approximately 0.75 nm. The permeability of the interstitial holes might be further reduced by the additional layers and would also help to mitigate effects of any defects in the lattice of the

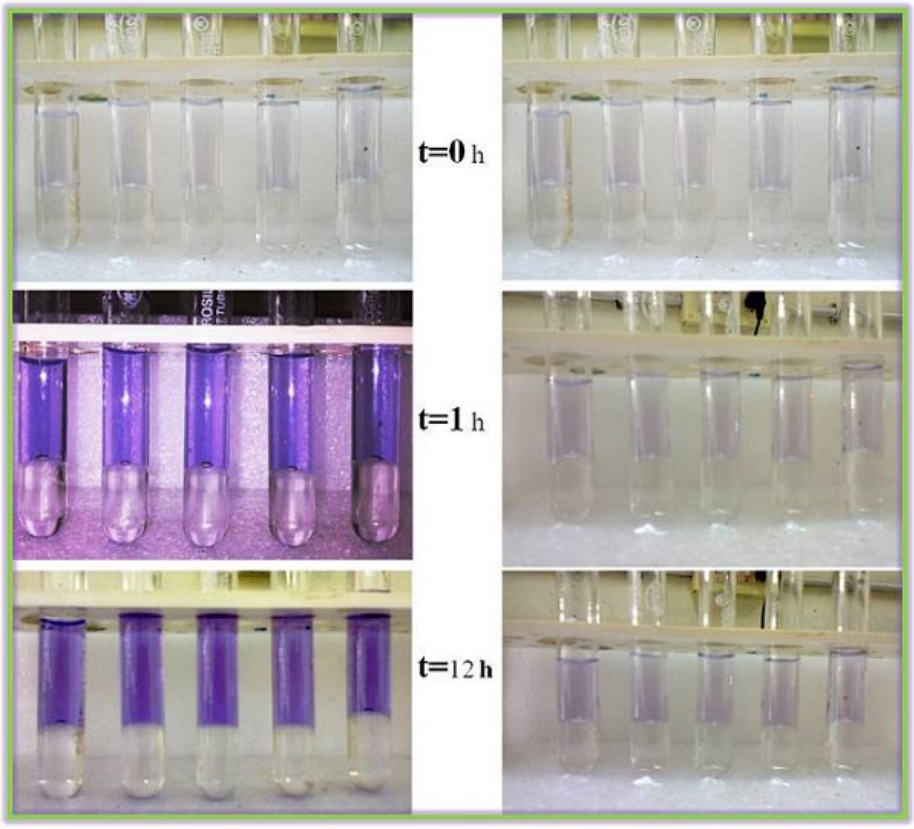

Figure 3.2.4. Digital camera photograph of diffusion of (left to right) glycine, alanine, valine, isoleucine and proline in (a) neutral and (b) charged state through the composite membrane at different time intervals.

particles. Thus, it is seen that the membrane allows the diffusion of amino acid molecules employed for this experiment. However, attempts made, so far, on nanomembrane filtration, emphasis has been given on nano-object filtration only without taking charge of the object into account (for uncharged nano-object filtration). To analyze the charge-dependence of the solute molecules to permeate across the membrane, five different amino acids, *viz.*, glycine, alanine,

valine, isoleucine and proline were employed to pass through the membrane under different pH conditions. The amino acid solutions are positive, neutral and negatively charged below, at and above the isoelectric point respectively.[48] In this experiment, we have taken pH = PI for neutral solution and pH = PI ± 0.5 for charged state in case of each amino acid. An aliquot of amino acid solutions of desired pH (adjusted prior to injection by adding buffer solutions prepared by mixing requisite amount of sodium acetate and acetic acid solutions; the overall ionic strength due to the addition of buffer solution is in the range of ~0.015 M) was injected into the CCl_4 layer by a syringe with a sharp needle through the side of the test tube and ninhydrin solution was added into the aqueous layer. The hole or channel created in this process will automatically be compensated up to large extent and would not affect the diffusion process seriously. The concentration of both amino acid and ninhydrin solution was maintained at 0.01 M, which is reported concentration for the reaction between amino acids and ninhydrin to take place exhibited by intense violet coloration of the solution.[49] Figure 3.2.4 shows the digital camera photograph of the permeation of both neutral and charged isoleucine molecules across the interface at different time intervals. It is seen that, at neutral condition, the diffusion of amino acid towards ninhydrin produces violet coloration after 1 h and gradually become intensified as the time progresses. On the other hand, in case of positively and negatively charged state, very faint coloration was observed even after 12 h. One important observation is that, in both positively and negatively charged states, there is no significant color change of the aqueous layer. The salient feature of physical significance is that in the case of other amino acid molecules, small size variation does not effect the rejection to a considerable extent. Blank experiments were performed at the same conditions (pH, buffer concentration) in which the amino acid was mixed with the ninhydrin. It is seen that color of the solution becomes blue in case of both charged and uncharged amino acids. Similar observation was noted in the case of different amino acids irrespective of their size. Another important observation is that, the trend of color change is same for both positively and negatively charged states. From these observations, it could be concluded that charge-dependent rejection has taken place due to dielectric exclusion, i. e., rejection of a charged species because of development of image charge at the metal-semiconductor interface of the membrane due to the presence of materials of different dielectric constants [33]. The interstitial spaces are sufficiently large so that the permeation of the amino acids is more dependent on the charge of the solutes rather than the size of the molecules.[50]

Under such a situation, the neutral species can only pass through the pores or channels of the membrane while the charged species get rejected at the interface.

3.2.4 Conclusion

In summary, 'thiol-ene' click chemistry has been exploited as a robust, efficient and orthogonal reaction to devise ultrathin membrane based on interfacial assembly of ligand-stabilised nanoparticles. Such plasmonic-semiconductor composite membrane has shown promise to exhibit charge-dependent permeability based on dielectric exclusion that opens up new avenues for targeted charged object separation. By tuning the nanoparticle composition and morphology, it would be possible to control size and shape selectivity and charge sensitivity of the membranes, making them promising materials for controlled encapsulation and filtration applications. Plasmonic and semiconductor nanoparticle-decorated composite membrane has been devised at the water-CCl_4 interface based on the self-assembly of ligand-stabilized gold and zinc oxide nanoparticles exploiting 'thiol-ene' click chemistry between the lateral thiol group of 11-mercapto undecanoic acid stabilized ZnO nanoparticles and ene functionality of the cinnamic acid attached to gold nanoparticles.The interfacial assembly of the ultrasmall particles develops a multilayer film at the interface that exhibit charge-dependent permeability of the amino acid molecules across the membrane. Such nanoparticle decorated multilayer membrane has been employed as charge dependent semipermeable membrane and can be a potential filter for separation of charged object from uncharged ones.

3.3 Water/Chloroform Interface-Mediated Fe_3O_4 Nanoparticle Membrane by Ligand Polymerization

3.3.1. Introduction

The fabrication of membranes via self-assembly of nanoscale materials is of interest for delivery vessels, size-selective separation and purification, controlled-release materials, sensors and catalysts, scaffolds for tissue engineering, low dielectric constant materials for microelectronic devices, antireflective coatings and proton exchange membranes for polymer electrolyte membrane fuel cells etc.[24,29,51,52] Recently, nanocrystalline iron oxides, composites and related materials have received special attention due to their viability as a platform for electrochemical, magnetic, and chemical biosensors.[53-54] While many kinds of nanoparticles, such as, metal, metal oxide and semiconductor nanoparticles have been used for constructing electrochemical sensors and biosensors, these nanoparticles play different roles in different sensing systems.[55] Since, the electrochemical detection is based on the current changes by modifying the electrode surface covered with a thin layer of particles due to the presence of chemical components of the reacting system, therefore, it has to make sure that, all the particles should be well-connected to each other so that the impulse could be transmitted throughout. Based on these conceptives, a robust and ultrathin membrane made up of nanoparticles could be aneffective choice for electrochemical sensing applications rather than, simply, attaching a layer of particles on the electrode surface. Such membrane-based electrochemical sensor is not only effective but also more sensitive than the conventional particle-based sensors,[56] while the fabrication of such membrane and draping it onto the electrode surface remain challenging.

L-Dopa is the immediate precursor of the neurotransmitter dopamine, that plays a very crucial role in the functioning of the central nervous, cardiovascular, renal, and hormonal systems, as well as in drug addiction and Parkinson's disease.[57] Thus, it becomes imperative for neuro and analytical scientists to find out a means to detect the presence of L-Dopa in human body up to trace amount.[58] Several techniques for the detection of L-Dopa have been described in the literature, including, flow injection method,[59] fluorescence spectroscopy,[60] cyclic voltammetry [61,62] and so on. While different types of membranes e. g., Nafion membranes,[63] enzyme collagen membranes,[64] bilayer lipid membranes,[65] gallium arsenide electrodes

functionalized with supported membranes[66] have, conventionally, been used for electrochemical sensing and nanoparticle-decorated ultrathin membrane have been employed to study their permeability and elasticity,[11] nanofiltration,[23] triggered release from liposomes,[67] targeted transfection[68] and so on; we have been interested to exploit nanoparticle-membrane as electrochemical sensor. In this section, we have reported the fabrication of Fe_3O_4 nanoparticle-decorated ultrathin membrane at the water/chloroform interface by terephthaloyl chloride and the membrane has been employed for electrochemical detection of L-Dopa up to nanomolar concentration.

3.3.2 Experimental

3.3.2.1 Synthesis of Fe_3O_4 Nanoparticles

Polyethylene glycol (PEG-13)-stabilized iron oxide nanoparticles were synthesized by modification of the procedure reported by Gillich *et al.*[69] In a typical synthesis, 1.99 g (0.01 mol) $(NH4)_2Fe(SO_4)_2.6H_2O$ and 5.41 g (0.02 mol) $FeCl_3.6H_2O$ were dissolved in 50 mL distilled water in a beaker so that the molar ratio of Fe^{2+} : Fe^{3+} = 1 : 2. In a separate beaker, an aqueous NH_4OH (30% v/v) solution (1.5 M) was prepared. Then, polyethylene glycol (0.1 M) was added at a ratio of 1 : 10 to both the above solutions to get precursor solutions I and II respectively. After that, precursor solution II was added to solution I dropwise under stirring condition at 40 ^0C; just after mixing the solutions, color of the solution changes from light brown to black indicating the formation of Fe_3O_4 nanoparticles. The stirring was continued for another 45 min and the solution was cooled to room temperature. The precipitate so-obtained was washed thrice by centrifugation and redispersed in distilled water. The particles are spherical or nearly spherical and the size of the particles was found to be 5 ± 0.5 nm.

3.3.2.2 Synthesis of the Membrane

Ultrathin membrane made up of PEG-coated Fe_3O_4 nanoparticles were synthesized at water/chloroform interface by intermolecular polymerization between pendant –OH groups of PEG anchored onto Fe_3O_4 nanoparticles surfaces with the help of terephthaloyl chloride, a well-known ligand cross-linker. In a typical method, 2 mL of Fe_3O_4 hydrosol (0.25 mM) was taken in a test tube and equal volume of chloroform containing small amount of terephthaloyl chloride

was mixed and shaken vigorously. After about 2 min, the mixture was allowed to settle and after few moments, the formation of a membrane has been observed at the interface.

3.3.2.3 Modification of the Gold Electrode with Nanoparticle-Decorated Membrane

The bare gold electrode was polished with 0.05 μm alumina powder and then, thoroughly, rinsed with distilled water. This, mechanically, cleaned gold electrode was, again, uncontaminated by repetitive cycling between potential -0.2 to +1.5 V *vs.* Ag/AgCl in 1.0 M H_2SO_4 solution until a stable characteristic cyclic voltammogram was obtained. The electrode was, then, rinsed with distilled water and clamped in such a manner that the gold surface is in contact with the Fe_3O_4 nanoparticle-decorated membrane formed at the water/chloroform interface. After 20 h keeping the solution undisturbed for overnight, the membrane modified gold electrode was formed and washed, thoroughly, with distilled water for further use.

3.3.2.4 Electrochemical Characterization of Membrane-Modified Electrode

The characterization of membrane-modified gold electrode was conducted using the redox probe $[Fe(CN)_6]^{3-/4-}$ as shown in Figure 3.3.1. Panel a shows the cyclic voltammogram of the bare electrode (black curve) and membrane-modified electrode (red curve) in 1.0 mM

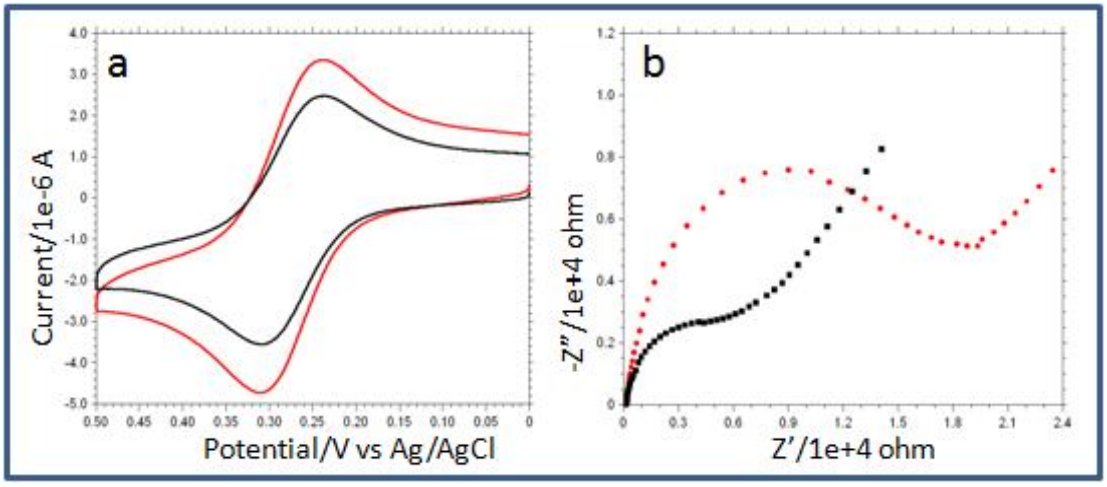

Figure 3.3.1. (a) Cyclic voltammogram and (b) electrochemical impedance spectroscopy of 1.0 mM $K_4[Fe(CN)_6]$ at bare (black curve) and Fe_3O_4 membrane-modified electrode (red curve) at pH=7.0.

$[Fe(CN)_6]^{3-/4-}$ in PBS at pH 7.0. For a bare gold electrode, the signature of a well-defined redox couple of $[Fe(CN)_6]^{3-/4-}$ was appeared with a peak-to-peak separation, ΔE_p = 74 mV. However, after modification with membrane, the peak current increased and peak-to-peak separation decreased, (ΔE_p = 63 mV) indicating successful modification of the electrode with the membrane. The Nyquist plot presented in panel b shows that after modification of the gold electrode, the charge transfer resistance (R_{CT}) decreased compared to bare gold electrode [R_{CT} (bare): 19056 Ω and R_{CT} (modified): 11004 Ω] which is due to monolayer formation over gold electrode surface. The surface coverage θ = 0.73, was obtained using, $\theta = [1 - (R_{ct}^0 / R_{ct})]$, where, R_{ct}^0 and R_{ct} are the charge transfer resistances of the redox probe at bare and membrane-modified gold electrodes, respectively, under similar conditions.

3.3.3. Results and Discussion

The structure and morphology of the membrane has been characterized by optical microscopy,

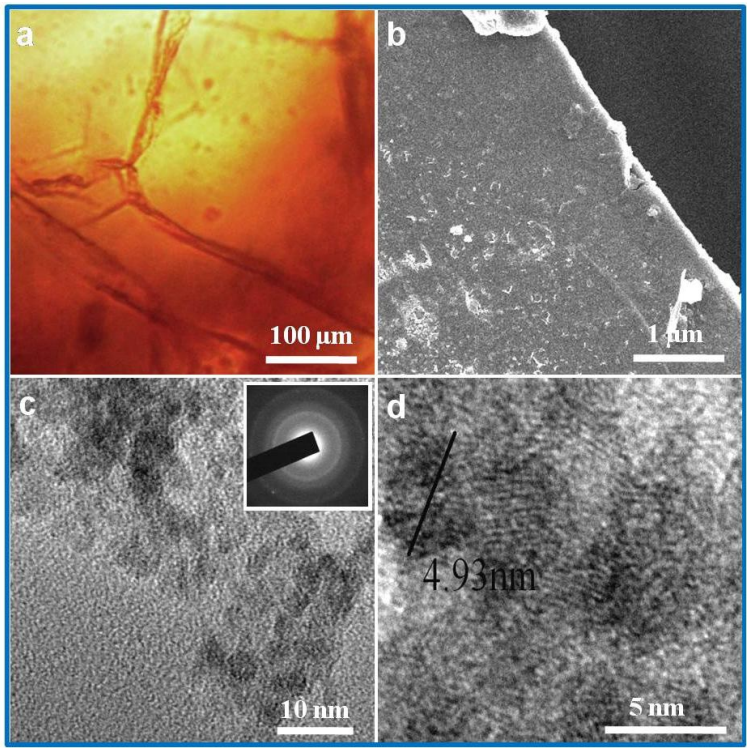

Figure 3.3.2. (a) Optical micrograph, (b) scanning electron micrograph, (c) transmission electron micrograph and (d) high resolution transmission electron micrograph of the Fe_3O_4 nanoparticle-decorated membrane. Inset in panel c shows the selected area electron diffraction pattern of the membrane.

scanning electron microscopy, transmission electron microscopy and high resolution transmission electron microscopic images as shown in Figure 3.3.2. Panel a shows the optical microscope image of the as-prepared membrane. The membrane so formed at the interface was collected by micropipette and kept suspended in chloroform in the cavity of a glass slide. An ultrathin membrane can, clearly, be observed; the ridges on the membrane arises during the transfer of the membrane by micropipette on the glass slide, which, in turn, support robustness of the membrane.[11] Typical SEM image of the membrane (panel b) exhibit the formation of an intact and robust membrane at water/chloroform interface.[76] Panel c is the representative transmission electron micrograph of the membrane which shows compact and regular monolayer arrangement of the nanoparticles in the membrane.[70] The selected area electron diffraction pattern shown in the inset exhibits five distinct diffraction rings of (220), (311), (420), (511)

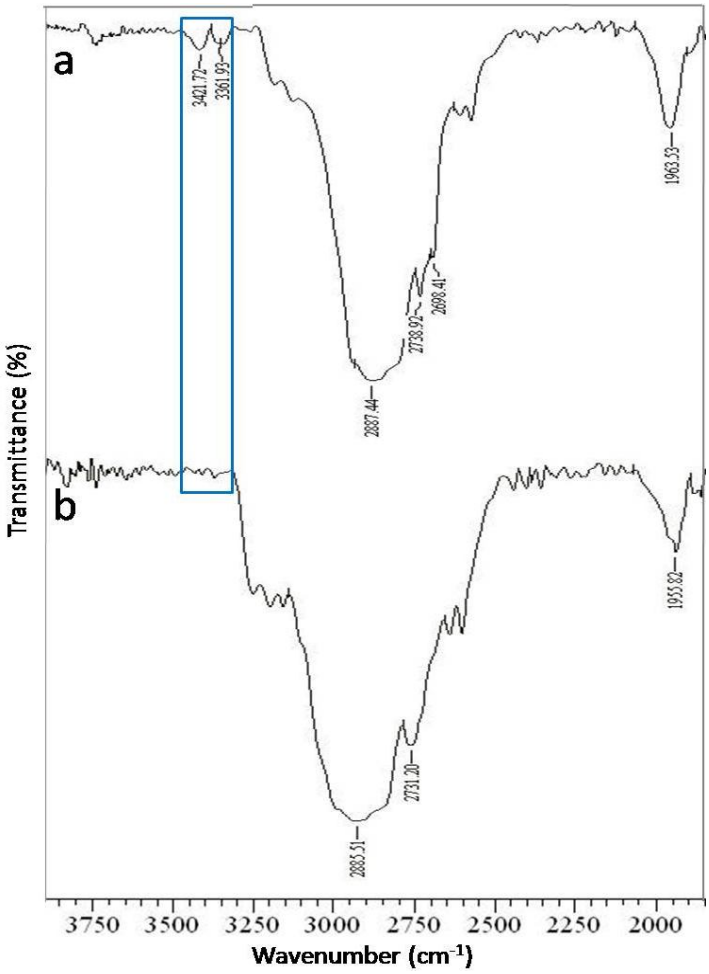

Figure 3.3.3. FTIR spectra of PEG-stabilized Fe_3O_4 nanoparticles (a) before and (b) after cross-linking.

and (440) confirmed a typical magnetite crystalline structure.[71] Panel d is the high resolution TEM image of the membrane which, further, confirms two dimensional ordering of the Fe_3O_4 nanoparticles in the membrane.[36]

The ligand cross-linking between the chain-end hydroxyl groups of PEG via terephthaloyl chloride has been monitored by FTIR spectroscopy. Figure 3.3.3 shows the overlaid FTIR spectra of PEG-13 stabilized Fe_3O_4 nanoparticles (trace a) and nanoparticle-decorated membrane formed after cross-linking (trace b). It is observed that, the peaks at *ca.* 3360 and 3420 cm^{-1} corresponding to –O–H stretching is disappeared indicating successful cross-linking between hydroxyl groups of PEG with the acyl chloride moiety of the terephthaloyl chloride molecules.[72]

It is well-established in the literature that ultrasmall particles strongly segregate to the interface of immiscible fluids, driven by a reduction of interfacial energy.[24,29,51] When such interfacial assembly of nanoparticles takes place in a 2D interface (a flat surface), thin films of nanoparticles could be produced in situ at interfaces between immiscible fluids. Such membranous structure may be less stable, but when the nanoparticles used in these interfacial assemblies are decorated with functional ligands, the assemblies can be stabilized and transformed into robust materials by performing chemistry on the functional groups contained within the ligand structure.[24,29] In this experiment, the PEG-13 stabilized Fe_3O_4 nanoparticle-decorated membrane at the water/chloroform interface has been stabilized by cross-linking the chain-end hydroxyl groups of PEG with two acyl chloride moieties of terephthaloyl chloride, as represented in Scheme 3.3.1.

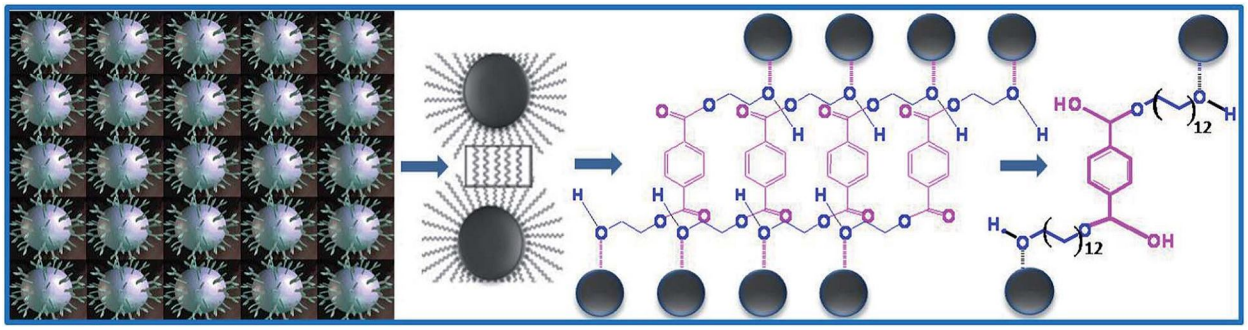

Scheme 3.3.1. Schematic presentation of formation of nanoparticle-decorated membrane by cross-linking of chain end hydroxyl groups of PEG with acyl chloride moiety of terephthaloyl chloride via ester linkage formation.

The magnetism of the membrane acquired, by virtue, of its magnetic nanoparticles as building blocks, was investigated by applying an external magnetic field (Figure 3.3.4). A

homogenous uniform membrane with over a large area (55.4 cm^2) is seen in the absence of the magnet (panel a). However, the membrane becomes folded towards a bar magnet when it is placed nearby and unfolded when the magnet bar is taken away. The membrane folding and unfolding is observed even up to ten cycles of operations pointing out the mechanical robustness of the membrane

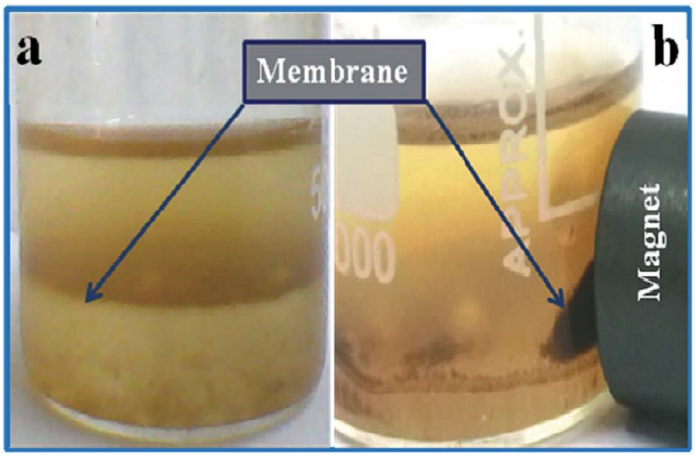

Figure 3.3.4. Response of the nanoparticle-decorated ultrathin membrane in the (a) absence and (b) presence of a bar magnet.

through magnetic actuation of super paramagnetic iron oxide nanoparticle membrane constituted of cross-linked ultrasmall particles. Amstad *et al.*[67] have demonstrated triggered release from reversibility of oxide nanoparticle containing membranes. Therefore, magneto-responsibility of the liposomes could be exploited in the near future for the development of efficient drug carriers that can deliver anticancer agents specifically into cancerous tissues exposed to a magnetic field.[24,52]

Now, the nanoparticle-decorated ultrathin membrane was employed as an electrochemical sensor for the determination of L-Dopa upto nanomolar concentration (Figure 3.3.5). The modification of the gold electrode with the membrane and its electrochemical characterization are described earlier. Panel a shows the cyclic voltammogram of 1.0 mM L-Dopa in 0.1 M PBS (pH 7.0) on bare (black curve) and membrane-modified gold electrode (red curve). The appearance of a pair of weak redox peak was observed with a peak-to-peak separation, ΔE_p = 230 mV on the bare gold electrode. However, a well-defined irreversible redox wave (ΔE_p = 188 mV) was seen on the modified electrode. It is noted that the anodic peak potential shifts

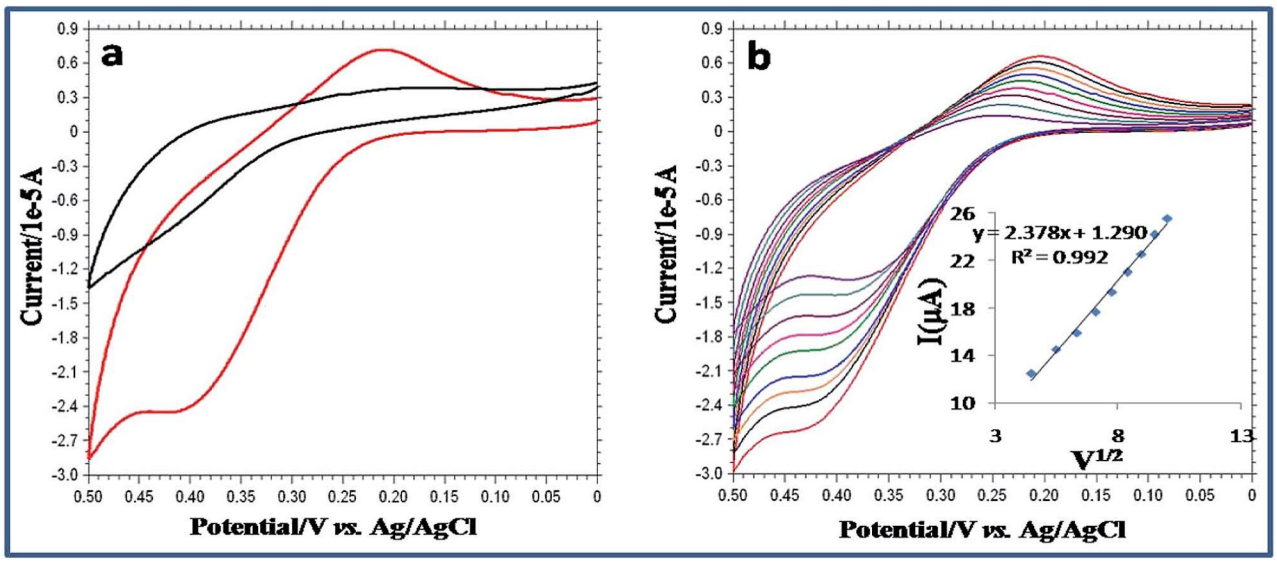

Figure 3.3.5. (a) Cyclic voltammogram of 1.0 mM L-Dopa (at pH ~ 7.0) at bare (black curve), and membrane-modified gold electrode (red curve); and (b) cyclic Voltametry of L-Dopa at different scan rate at membrane-modified gold electrode.

negatively (26 mV) and the anodic peak current is higher (15 mA) in comparison with the bare lectrode, which suggests that the membrane-modified gold electrode shows electrocatalytic oxidation of L-Dopa (L-Dopa + $2H_2O$ → Dopaquinone + $4H^+$ + 4e). The transfer of four electrons for L-Dopa oxidation was confirmed by comparing the current height with the $[Fe(CN)_6]^{3-/4-}$ redox couple under similar measurement conditions.[73] The scan rate dependence of oxidation current of L-Dopa is proportional to the square root of the scan rate indicating that the oxidation is diffusion-controlled.[74] Panel b shows the cyclic voltammetric responses of the membrane modified electrode for L-Dopa at different scan rate. Inset shows a plot of oxidation current with increase in concentration of L-Dopa. It is seen that, the oxidation current of L-Dopa increases, linearly, with increase in concentration in the range of 1–4.5 mM. The concentration of L-Dopa could be determined in the range 0.05–10 mM and the limit of detection (LOD, an average of three determinations) was obtained as 9.5 nM using equation 3s/m, where, s is the standard deviation of the measurement and m is the slope of the calibration curve, I_p (mA) = 0.122C (mM) + 6.608 and R^2 = 0.996. A comparative account of the sensing capabilities for the determination of L-Dopa in the presence of different materials and methods is shown in the Table 3.3.1.

Table 3.3.1. Comparative Account of the Sensing Capabilities for the Determination of L-Dopa in the Presence of Different Materials and Methods

Materials	Method	Concentration range (μM)	LOD (μM)	Reference
Oxovanadium-salen complex	flow injection method	1-100	0.80	Teixeira *et al.* [Ref. 11]
Phenylboronic acid derivative of lucifer yellow	fluorescence spectroscopy	0-5000	–	Coskun *et al.* [Ref. 12]
Chloro(pyridine) bis(dimethylglyoximato) cobalt(III)/multi-walled carbon nanotube	cyclic voltammetry	3-100	0.86	Leite *et al.* [Ref. 13]
Cobalt hexacyanoferrate/ large mesopore carbon composite modified electrode	cyclic voltammetry	0.1-1900	0.02	Yan *et al.* [Ref. 14]
Fe_3O_4 membrane	cyclic voltammetry	0.05-10	0.01	Present work

Moreover, it is seen that nanoparticle-decorated membrane is able to determine L-Dopa and ascorbic acid in binary mixtures of the compounds, linearly, in an appreciable concentration range. Therefore, it could be inferred that, the nanoparticle-decorated membrane could, even, be exploited as an electrochemical sensor for simultaneous determination of L-Dopa and ascorbic acid in a binary mixture of the compounds.

L-Dopa has been detected by membrane-modified electrode at different pH to investigate the effect of pH on sensing (Figure 3.3.6). At pH 7.0, the interaction between membrane-modified gold electrode and L-Dopa (exists as negatively charged at this pH) is maximum as shown by the profile showing the variation of peak current as a function of pH. Below or above pH 7.0, the interaction is less because L-Dopa exists in zwitterionic form at pH 5.0 (isoelectric point, pI = 5.2) and doubly negatively charged at pH >>7.0. Therefore, it is evident that, the electrostatic interaction between L-Dopa and membrane-modified electrode surface is less as apparent from the low anodic current height in the cyclic voltammogram.

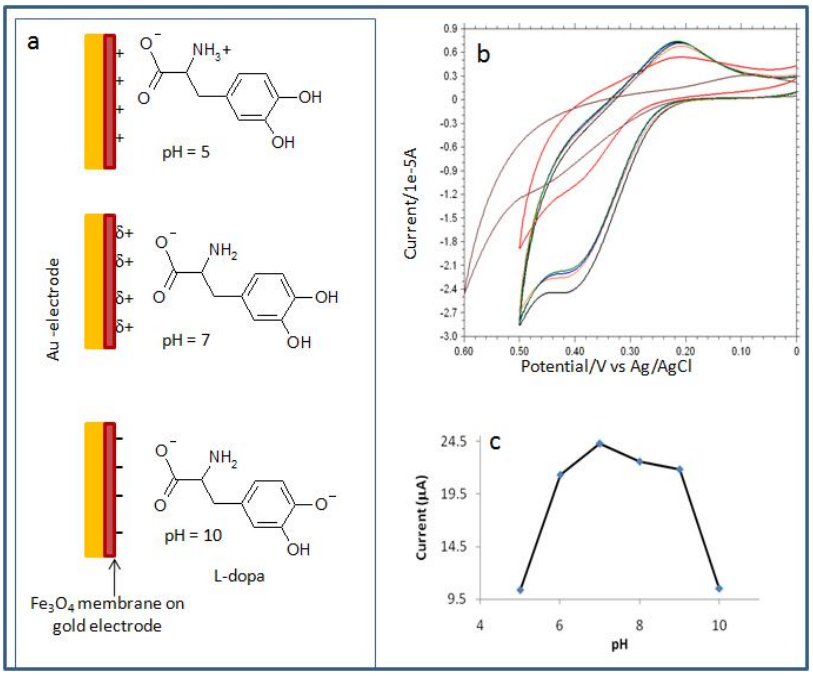

Figure 3.3.6. (a) Schematic presentation of L-Dopa and its interaction with membrane-modified gold electrode (b) cyclic voltammogram of L-Dopa at membrane modified gold electrode at different pH. [pH= 5.0 (violet); 6.0 (green); 7.0 (black); 8.0 (pink); 9.0 (blue); 10.0 (red)] (c) plot of pH *vs.* peak current of L-Dopa at membrane-modified gold electrode.

Simultaneous detection of L-Dopa and ascorbic acid (AA) in binary mixtures was studied at membrane-modified gold electrode. Figure 3.3.7 shows the overlaid differential pulse voltametry obtained for a L-Dopa and AA mixture at membrane-modified electrode in PBS (pH = 7.0) by changing the concentration of both L-Dopa and AA (1, 2, 3, 4, 5, 6 µM). The oxidation peaks of L-Dopa (0.38 V) and AA (0.24 V) with a peak separation of 140 mV was observed with increasing the concentration of both compounds. The regression equation for L-Dopa and AA was found to be, I_p (µA) = 0.2217 C (µM) + 6.1231 and I_p (µA) = 0.2254 C (µM) + 1.8549, respectively in the range of (1- 6 µM). The current responses of both L-Dopa and AA, linearly, increase with a correlation coefficient of 0.998 and 0.999, respectively. Therefore, it could be inferred that, the nanoparticle-decorated membrane could be employed as an electrochemical sensor for simultaneous determination of L-Dopa and ascorbic acid in a binary mixture of the compounds.

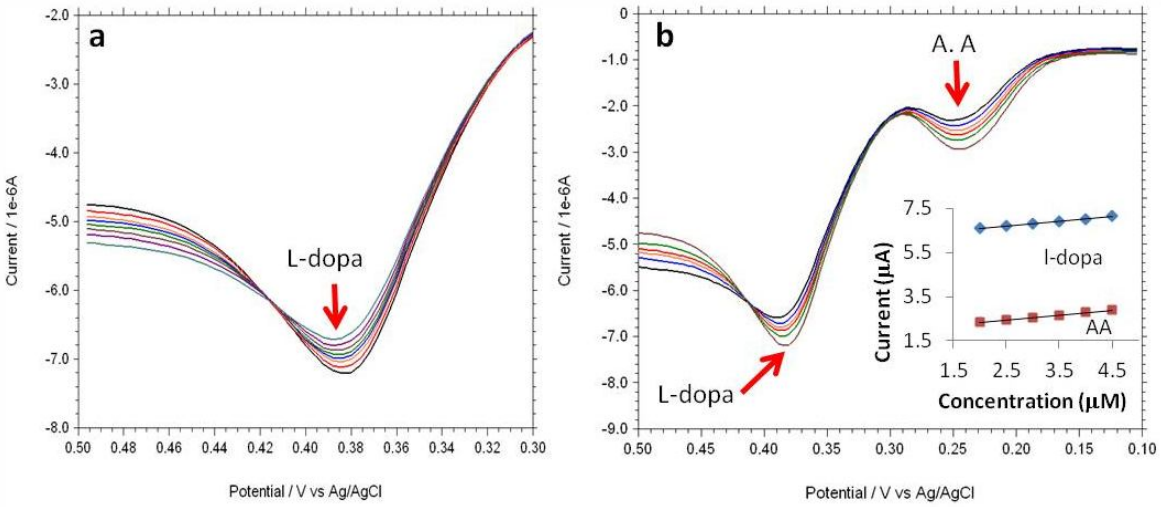

Figure 3.3.7. (a) Differential pulse voltametry of L-Dopa in different concentrations: (a) 1.0, (b) 1.5, (c) 2.0, (d) 2.5, (e) 3.0, (f) 3.5, (g) 4.0 and (h) 4.5 µM; and (b) overlaid differential pulse voltametry of L-Dopa and ascorbic acid in different concentrations. Inset shows the plots of current (µA) *vs.* concentration (µM) of L-Dopa and ascorbic acid.

3.3.4 Conclusion

In summary, water/chloroform interface has been exploited as a viable platform for the fabrication of Fe_3O_4 nanoparticledecorated robust, ultrathin membrane by cross-linking the chain-end hydroxyl groups of PEG ligands attached onto nanoparticle surface with the help of terephthaloyl chloride as the ligand cross-linker. This nanoparticle-decorated ultrathin membrane has been, successfully, employed for electrochemical detection of L-Dopa (and also L-Dopa and ascorbic acid simultaneously) up to nanomolar level concentrations. The membrane could be manipulated in the near future using external magnetic field, providing a convenient and gentle means to utilise as efficient delivery vehicles for various therapeutic agents, particularly, in cancer therapy. poly(ethyleneglycol) (PEG-13)-stabilised magnetic Fe_3O_4 nanoparticle decorated ultra-thin membrane has been devised at the water/chloroform interface by ligand cross-linking between pendant hydroxyl groups of PEG with terephthaloyl chloride. This robust nanoparticle-decorated membrane has been employed as an electrochemical sensor for the detection of L-Dopa up to nanomolar concentration.

References

(1) Lasic, D. D. In *Liposomes*: *Physics to Applications, Elsevier*, Amsterdam, 1993.

(2) Pickering, S. U. *J. Chem. Soc. Trans.* 1907, 91, 2001–2021.

(3) Pieranski, P. *Phys. Rev. Lett.* **1980,** *45*, 569–572.

(4) Dinsmore, A. D.; Hsu, M. F.; Nikolaides, M. G.; Marquez, M.; Bausch, A.; Weitz, D. A. *Science* **2002,** *298*, 1006–1009.

(5) Lanza, R. P.; Langer, R.; Vacanti, J. In *Principles of Tissue Engineering*, Academic Press, San Diego, CA, 2000.

(6) Morris, R. E. *Nature Chem.* **2011,** *3*, 347–348.

(7) Korgel, B. A. *Nature Mater.* **2010,** *9*, 701–703.

(8) Timoshenko, S.; Woinowsky-Krieger, S. In *Theory of Plates and Shells*, McGraw Hill: New York, 1987.

(9) Simkiss, K.; Wilber, K. M. In *Biomineralization*, Academic Press, London, 1980.

(10) Stookey, D. J. In *Membrane Technology in the Chemical Industry*, Nunes, S. P. and Peinemann, K. V. Eds.: Wiley-VCH, New York, Ch. 8, **2001**.

(11) Lin, Y.; Skaff, H.; Böker, A.; Dinsmore, A. D.; Emrick, T.; Russell, T. P. *J. Am. Chem. Soc.* **2003**, *125*, 12690–12691.

(12) Kumar, A.; Mandal, S.; Mathew, S. P.; Selvakannan, P. R.; Mandale, A. B.; Chaudhari, R. V.; Sastry, M.; *Langmuir* **2002,** *18*, 6478–4683.

(13) Duan, H.; Wang, D.; Kurth, D. G.; Möhwald, H. *Angew. Chem. Int. Ed.* **2004**, *43*, 5639–5642.

(14) Arumugam, P.; Patra, D.; Samanta, B.; Agasti, S. S.; Subramani, C.; Rotello, V. M. *J. Am. Chem. Soc.* **2008**, *130*, 10046–10047.

(15) He, J.; Kanjanaboos, P.; Frazer, N. L.; Weis, A.; Lin, X. -M.; Jaeger, H. M. *Small*, **2010**, *6*, 1449–1456.

(16) Shi, W.; Sahoo, Y.; Swiharta, M. T. *Colloids Surf. A* **2004**, *246*, 109–113.

(17) Pal, A.; Ghosh, S. K.; Esumi, K.; Pal, T. *Langmuir* **2004**, *20*, 575–578.

(18) Ghosh, S. K.; Nath, S.; Kundu, S.; Esumi, K.; Pal, T. *J. Phys. Chem. B* **2004**, *108*, 13963–13971.

(19) Ghosh, S. K.; Pal, T. *Chem. Rev.* **2007**, *107*, 4797–4862.

(20) Song, H. Y.; Oh, S. W.; Moon, S. D.; Kang, Y. S. *J. Colloid Interface Sci.* **2007**, *314*, 683–688.

(21) Hasan, M.; Bethell, D.; Brust, M. *J. Am. Chem. Soc.* **2002**, *124*, 1132–1133.

(22) Chen, S.; Yao, H.; Kimura, K. *Langmuir* **2001,** *17*, 733–739.

(23) He, J.; Lin, X.; Chan, H.; Vukovic, L.; Kral, P.; Jaeger, H. M. *Nano Lett.* **2011**, *11*, 2430–2435.

(24) Wang, D.; Möhwald, H. *J. Mater. Chem.* **2004**, *14*, 459–468.

(25) Whitesides, G. M.; Grzybowski, B. **2005**, *295*, 2418–2421.

(26) Wilcox, D. L. *Hollow and Solid Spheres and Microspheres: Science and Technology Associated with their Fabrication and Application*, 1995, Vol. 372, Materials Research Society, Pittsburgh, Pennsylvania.

(27) Vriezema, D. M.; Aragones, M. C.; Elemans, J. A. A. W.; Cornelissen, J. J. L. M.; Nolte, A. E. R. J. M. *Chem. Rev.* **2005**, *105*, 1445–1489.

(28) Binder, W. H. *Angew. Chem. Int. Ed.* **2005**, *44*, 5172–5175.

(29) Böker, A; He, J.; Emrick, T.; Russell, T. P. *Soft Matter* **2007**, *3*, 1231–1248.

(30) Kolb, H. C.; Finn, M. G.; Barry Sharpless, K. *Angew. Chem. Int. Ed.* **2001**, *40*, 2004–2021.

(31) Meldal, M.; Tornøe, C. W. *Chem. Rev.* **2008**, *108*, 2952–3015.

(32) Stevens, M. P. *Polymer Chemistry*, 1999, 3rd ed., Oxford University Press: Oxford, New York, pp. 208–209.

(33) Hoyle, C. E.; Bowman, C. N. *Angew. Chem. Int. Ed.* **2010**, *49*, 1540–1573.

(34) Lowe, A. B. *Polym. Chem.* **2010**, *1*, 17–36.

(35) Northrop, B. H.; Coffey, R. N. *J. Am. Chem. Soc.* **2012**, *134*, 13804–13817.

(36) Samanta, B.; Patra, D.; Subramani,; Ofir, C.; Yesibug, Y. G.; Sanyal, A.; Rotello, V. M. *Small* **2009**, *5*, 685–688.

(37) Pacholski, C.; Kornowski, A.; Weller, H. *Angew. Chem. Int. Ed.* **2002**, *41*, 1188–1191.

(38) Wang, L.; Wei, G.; Sun, L.; Liu, Z.; Song, Y.; Tao, Y.; Sun, Y.; Guo, L.; Li, Z. *Nanotechnology* **2006**, *17*, 2907–2912.

(39) Binks, B. P. *Curr. Opin. Colloid Interface Sci.* **2002**, *7*, 21–41.

(40) Luther, J. M.; Jain, P. K.; Ewers, P.; Alivisatos, A. P. *Nature Mat.* **2011**, *10*, 361–366.

(41) Ghosh, S. K.; Pal, T. *Chem. Rev.* **2007**, *107*, 4797–4862.

(42) Abu-Eittah, R. H.; Khedr, M. K.; Goma, M.; Zordok, W. *Int. J. Quantum Chem.* **2012**, *5*, 1256–1272.

(43) Munechika, K.; Chen, Y.; Tillack, A. F.; Kulkarni, A. P.; Plante, I. J. L.; Munro, A. M.; Ginger, D. S. *Nano Lett.* **2010**, *10*, 2598–2602.

(44) Murray, C. B.; Kagan, C. R.; Bawendi, M. G. *Annu. Rev. Mater. Sci.* **2000**, *30*, 545–610.

(45) Glogowski, E.; Tangirala, R.; He, J.; Russell, T. P.; Emrick, T. *Nano Lett.* **2007**, *7*, 389–393.

(46) Mellor, J. W. *A Comprehensive Treatise on Inorganic and Theoretical Chemistry*, 1923, Longmans Green and Co, London.

(47) Wang, D.; Duan, H.; Möhwald, H. *Soft Matter* **2005**, *1*, 412–416.

(48) Lehninger, A. L. In *Principles of Biochemistry*, Nelson, D. L.; Cox. M. M. Eds., 4th edn., 2004.

(49) Harding, V. J.; Warneford, F. H. S. *J. Biol. Chem.* **1916**, *25*, 319–335.

(50) Rabin, Y.; Tanaka, D. M. *Phys. Rev. Lett.* **2005**, *94*, 148103 1–4.

(51) Binder, W. H. *Angew. Chem. Int. Ed.* **2005**, *44*, 5172–5175.

(52) van Rijn, P.; Tutus, M.; Kathrein, C.; Zhu, L.; Wessling, M.; Schwaneberg U.; Böker, A. *Chem. Soc. Rev.* **2013**, *42*, 6578–6592.

(53) Laurent, S.; Forge, D.; Port, M. ; Roch, A.; Robic, C.; Vander Elst, L.; Muller, R. N. *Chem. Rev*. **2008**, *108*, 2064–2110.

(54) Urbanova, V.; Magro, M.; Gedanken, A.; Baratella, D.; Vianello, F.; Zboril, R. *Chem. Mater*. **2014**, *26*, 6653–6673.

(55) Pumera, M. In *Nanomaterials in Electrochemical Sensing and Biosensing*, CRC Press, Boca Raton, USA, 2013.

(56) Luo, X.; Morrin, A.; Killard, A. J.; Smyth, M. R. *Electroanalysis* **2006**, *18*, 319–326.

(57) Damier, P.; Hirsch, E. C.; Agid, Y.; Graybiel, A. M. *Brain* **1999**, *122*, 1437–1448.

(58) Venton, B. J.; Wightman, R. M. *Anal. Chem.* **2003**, *224*, 414A–421A.

(59) Teixeira, M. F. S.; Marcolino-Júnior, L. H.; Fatibello-Filho, O.; Dockal M´arcio, E. R.; Bergamini, F. *Sens. Actuators* B, **2007**, *122*, 549–555.

(60) Coskun, A.; Akkaya, E. U. *Org. Lett.* **2004**, *6*, 3107–3109.

(61) Leite, F. R.; Maroneze, C. M.; de Oliveira, A. B.; dos Santos, W. T.; Damos, F. S.; Silva, C. L. R. *Bioelectrochemistry* **2012**, *86*, 22–29.

(62) Yan, X.; Pan, D.; Wang, H.; Bo, X; Guo, L. *J. Electroanal. Chem*. **2011**, *663*, 36–42.

(63) Mercado, R. C.; Moussy, F. *Biosens. Bioelectron*. **1998**, *13*, 133–145.

(64) Thevenot, D. R.; Sternberg, R.; Coulet, P. R.; Laurent, J.; Gautheron, D. C. *Anal. Chem.* **1979**, *51*, 96–100.

(65) Nikolelis, D. P.; Krull, U. J. *Electroanalysis*, **1993**, *5*, 539– 545.

(66) Gassull, D.; Ulman, A.; Grunze, M.; Tanaka, M. *J. Phys. Chem. B* **2008**, *112*, 5736–5741.

(67) Amstad, E.; Kohlbrecher, J.; Müller, E.; Schweizer, T.; Textor, M.; Reimhult, E. *Nano Lett.* **2011**, *11*, 1664–1670.

(68) Delcea, M.; Sternberg, N.; Yashchenok, A. M.; Georgieeva, R.; Bäumler, H.; Möhwald, H.; Skirtach, A. G. *ACS Nano* **2012**, *6*, 4169–4180.

(69) Gillich, T.; Acikgöz, C.; Isa, L.; Schlüter, A. D.; Spencer, N. D.; Textor, M. ; *ACS Nano* **2013**, *7*, 316–329.

(70) Ali, M.; Bora, S.; Ghosh, S. K. *Langmuir* **2014**, *30*, 10449–10455.

(71) Cornell, R. M.; Schwertmann, U. In *The Iron Oxides*, VCH, Weinheim, 2nd edn, 2003.

(72) Hussain, S. T.; Iqbal, M.; Mazhar, M. *J. Nanopart. Res.* **2009**, *11*, 1383–1391.

(73) Spencer, J. P. E.; Jenner, P. ; Daniel, S. E.; Lees, A. J.; Marsden, D. C.; Halliwell, B.; *J. Neurochem*. **1998**, *71*, 2112–2122.

(74) Mazloum-Ardakani, M.; Yavari, M.; Ali Sheikh-Mohseni, M.; Mirjalili, B. F. *Catal. Sci. Technol.* **2013**, *3*, 2634**–**2638.